Nitridation and CVD Reactions with Hydrazine

Kirkland W. Vogt and Paul A. Kohl
School of Chemical Engineering, Georgia Institute of Technology, Atlanta, GA 30332

Joseph A. Abys
AT&T Bell Laboratories, Murray Hill, NJ 07974

The low-temperature nitridation of gallium arsenide, silicon and transition metals was investigated using hydrazine. Gallium nitride films were grown on gallium arsenide (GaAs) by direct reaction of the semiconductor surface layers with hydrazine at 200–400°C. Auger electron spectroscopy and X-ray photoelectron spectroscopy (XPS) analyses show that the films are primarily gallium nitride with a small oxide impurity. Thin nitride films (~15 Å) were grown on silicon by reaction with hydrazine at 300–500°C. Ellipsometry results suggest that the film growth goes through different phases following linear, parabolic and logarithmic functions with time. XPS analysis shows that the nitride films could be formed at much lower temperatures than possible with ammonia (300 vs. 600°C). The formation of numerous transition metal nitrides (Co, Cr, Fe, Mo, Si, Ta, Ti, V, and W) by reaction with hydrazine at 400°C is demonstrated, as well as the chemical vapor deposition of boron nitride films from diborane and hydrazine reactants. The temperature at the mixing point was critical in determining the final composition of the film. A 1-D transport model suggests that the reaction rate at 400°C was kinetically limited. The results also agree qualitatively with thermodynamic equilibrium calculations.

Introduction

Nitride films are attractive surface layers because they often have high melting points, excellent hardness, valuable electrical properties, and good chemical stability (Weast, 1980; Vasile et al., 1990; Lee et al., 1990). For example, the exposed surfaces of many metals are susceptible to corrosion. Stabilizing the surface with a nitride is helpful in minimizing damage to the metal substrates (Maissel and Glang, 1970). Silicon nitride is used in the manufacture of transistors and capacitors in integrated circuits (Runyan and Bean, 1990; Murarka et al., 1979a).

A more specific application of metal nitrides is the passivation of III–V semiconductors. An attractive passivation process would mimic the growth of silicon dioxide on silicon. Because the oxide film grows by consumption of the silicon substrate, the film/substrate interface is clean, and the film provides excellent passivation. In the case of III–V semiconductors, a thin, large bandgap semiconductor would first be grown on the surface by consuming the surface layers of the III–V semiconductor substrate. The direct growth process would react the surface with gas species. The film/substrate interface is expected to be very clean because atmospheric and other surface impurities would not be present. Since the energy gap of the passivating material is wider than the semiconductor, a potential barrier would be created that repels both holes and electrons from the insulator (Pankove, 1980). The decreased concentration of free carriers would help minimize the effect of any surface states. Although this approach of using large bandgap materials for passivating III–V semiconductors is attractive, it does not preclude the possibility of other problems occurring, such as interface states and defects.

Unfortunately, passivation of III–V semiconductor surfaces is difficult. Oxidation produces hydroscopic, noninsulating films that are not suitable for microelectronics applications (Thurmond et al., 1980; Capasso and Williams, 1982; Frese and Morrison, 1979; Chang et al., 1978; Hall et al., 1986; Schwartz et al., 1979; Wang et al., 1982). Additionally, III–V semiconductors have high vapor pressures and require

Correspondence concerning this article should be addressed to P. A. Kohl.

processing below 400°C (Kang et al., 1987). Nitridation with ammonia or nitrogen requires temperatures in excess of 800°C (Faulkner et al., 1970; Isherwood and Wickenden, 1970; Prochazkova and Srobar et al., 1977; Matsuno et al., 1980). Plasma, ion, and photon beams can lower the nitridation reaction temperature, but high-energy particles and photons in these processes can damage the surface layers of the crystalline semiconductors (Gourrier et al., 1983, 1985; Friedel and Landesman, 1987; Blanchet et al., 1984; Berger et al., 1990; Troost et al., 1991; Sawada et al., 1987; Guizot et al., 1989).

This study investigated the direct nitridation of GaAs with hydrazine as a possible passivation process. A nitride film was grown by consuming the native semiconductor through reaction with hydrazine. The endothermic nature of hydrazine lowers the amount of thermal energy necessary for the growth and deposition of nitride films (Schmidt, 1984). Group III nitrides are stable compounds that can chemically and electrically passivate the semiconductor surface.

Once the semiconductor lattice has been terminated with a wider bandgap material (GaN), a thick insulator can be deposited on the surface. The interface between the large bandgap semiconductor and the insulator is not as sensitive to dangling bonds because the potential barrier is larger (Pankove et al., 1983). Although the potential barrier is important, the presence of charged states (or other defects) at the interface can dominate the electrical properties. In this investigation, boron nitride has been investigated as the insulator layer. Boron nitride films have good insulating properties, high melting points, and high resistivities making them attractive for use in the microelectronics industry (Rand and Roberts, 1968). They have been used as interlayer dielectrics in very large-scale integration (VSLI) devices and as the active insulating layer for metal–insulator–metal devices in switching arrays for liquid-crystal displays (Strongin et al., 1992). Boron nitride films can also be used as electron and X-ray lithography masks (Levy et al., 1988; King et al., 1987). Boron nitride films have been prepared previously by the reaction of ammonia and boron trichloride at 250–1,200°C (Motojima et al., 1982; Sano and Aoki, 1981), reaction of ammonia and diborane at 250–1,250°C (Rand and Roberts, 1968; Murarka et al., 1979; Adams and Capio, 1980; Kim et al., 1984), reaction of diborane and ammonia in a plasma (Gafri et al., 1980; Hyder and Yep, 1976), pyrolysis of borazine at 300–450°C (Adams, 1981), reaction of decaborane and ammonia at 300–800°C (Nakamura, 1985), and metal-organic chemical vapor deposition (MOCVD) from triethylboron and ammonia at 750–1,200°C (Nakamura, 1986). More recently, Rodriguez et al. (1992) and Truong et al. (1992) have studied the adsorption kinetics of diborane, ammonia, and hydrazine on ruthenium. The results of these UHV studies suggested that high reaction temperatures (> 600°C) were needed to form boron nitride films because ammonia has high chemical stability. The motivation in this work is to lower the reaction temperature (< 400°C) by using a less stable nitrogen species, namely hydrazine.

In summary, the low-temperature nitridation of GaAs, silicon, and transition metals using hydrazine has been studied. The investigation included the design and construction of a reactor, development of a process sequence, chemical analysis of the nitride films, and modeling for the nitride film growth behavior. The second type of reaction considered was the chemical vapor deposition (CVD) of boron nitride films from diborane and hydrazine. The study included thermodynamic equilibrium calculations, transport modeling, and experimental analysis.

Experimental

Analysis equipment

Auger Electron Spectroscopy (AES) and X-ray Photoelectron Spectroscopy (XPS) were used for elemental analysis of the thin films. AES was performed with a Physical Electronics Model 600 (Eden Prairie, MN) Scanning Auger Multiprobe. The base pressure inside the chamber was $\sim 7.0\times 10^{-10}$ torr. A 3-keV, 1-μA electron beam was used for excitation. A rastered 2-keV (40-$\mu A/cm^2$) Ar^+ ion beam was used during ion etching. The argon pressure was $\sim 1.0\times 10^{-8}$ torr. The ion etch rate was 60 ± 15 Å/min for thermally grown SiO_2. The variation in ion etch rates between the different substrates was not investigated in this study. The Surface Science SSX-100 (Mountain View, CA) XPS was equipped with an aluminum K-α X-ray source and a crystalline X-ray monochromator. The operating pressure in the sample chamber was $\sim 4\times 10^{-9}$ torr. The XPS system was also equipped with a 4-keV argon ion gun that was used to lightly clean the surface. The argon pressure was 3.7×10^{-7} torr during ion etching. The ion etch rate was 15 ± 5 Å/min for thermally grown SiO_2. The spectrometer was calibrated to Au $4f_{7/2}$ at 84.0 eV, and the peak positions were referenced to C1s at 284.6 eV. Standard materials were analyzed whenever possible to identify oxidation states, stoichiometry, and charging effects.

Film thicknesses were measured with a *Plasmos SD 2300* ellipsometer. For silicon nitride, the refractive index of the film was assumed constant at 2.0. Each measurement was the average of ten scans.

Reactor design

Since reactions with hydrazine and diborane pose some safety and handling concerns (Crowl and Louvar, 1990), extra effort was used to design and construct the reaction system illustrated in Figure 1. The reactant gases were ultrahigh purity (UHP) argon and a mixture of 850-ppm diborane in UHP argon. The gases were fed into the nitride reactor with a gas-handling system constructed with electro-polished stainless steel tubing, Cajon (Macedonia, OH) VCR fittings, and butt-coupled arc welds. This provided the highest possible cleanliness and the lowest leakage rates. The entire gas-handling system had a leak rate of less than 1×10^{-9} cc/s at 50 mtorr, as measured with a mass spectrometer/helium-leak test. At each cylinder, Cajon "E4" excess-flow valves prevented a catastrophic leak in the event of a ruptured line. Cajon "CW" check valves presented accidental mixing of the gases and backflow. Point-of-use purification helped minimize oxygen, water, and particle contamination in the reactant gases. Each gas line had a Matteson (Secaucus, NJ) 0.01-μm particle filter to reduce the particle contamination of the reactant gases below 1 ppb. The argon line had an MG Industries (Valley Forge, PA) "Oxisorb" gas purification system to remove oxygen and water and produce the highest possible

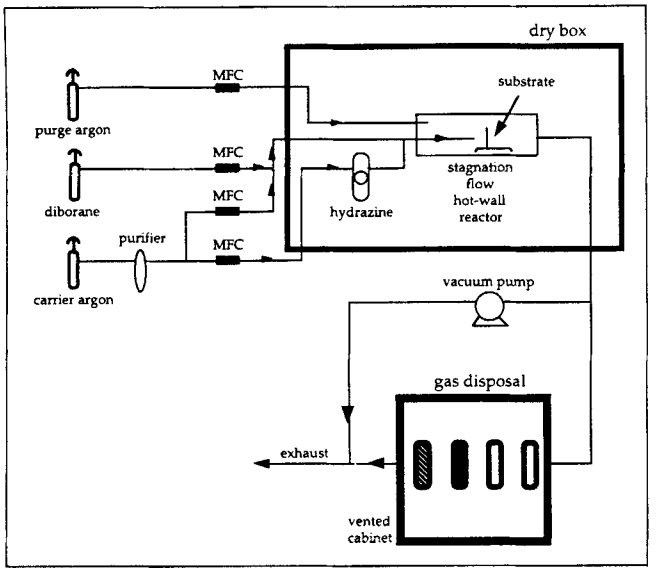

Figure 1. Reactor configuration.

purity of gas prior to reaction. Mass flow fluctuations of the gases were minimized with Brooks 5850 (Hatfield, PA) and Tylan FC 260 (Carson, CA) mass flow controllers, and a Tylan RO-28 power supply. The gases were piped into a Vacuum Atmospheres (Hawthorne, CA) HE series inert atmosphere dry box that had less than 2 ppm oxygen and water contamination. The tube reactor was placed inside the inert atmosphere dry box. The dry box provided a safety containment chamber for the hydrazine during loading, use, and storage. Hydrazine is more stable in nitrogen than air, and the dry box eliminated undesirable human contact. Olin (Stamford, CT) "Ultra-pure" hydrazine, 99.7% by weight, was introduced into the reactor with a bubbler and argon carrier gas, where the argon flow rate and temperature (that is, vapor pressure) controlled the mass flow rate of the hydrazine entering the reactor. The argon flow rate and hydrazine temperature were controlled with a Brooks 5850 mass flow controller and VWR 1130 constant temperature bath, respectively. In some cases, activated alumina was used to improve the purity of the hydrazine as discussed by Good and Poole (1971). Powdered activated alumina (particle diameter 0.125–0.25 mm) was vacuum-dried at 1×10^{-6} torr for four days at 120°C. The dried alumina was mixed with as-received 99.7% hydrazine and allowed to sit for 7 days. Since the bath was in the dry box, a nonaqueous heat-transfer fluid, Dow Corning "Syltherm XLT" was used. Because hydrazine can decompose rapidly on many metals (Schmidt, 1984), Pyrex lines and valves were used to transport the hydrazine vapor into the reactor. The lines were heated with heat tape to prevent condensation before entering the reactor. The reactant gases were injected into the center of the 3-in. dia., 40-in.-long Pyrex glass reactor with an injection tube. The injection tube mixed the reactant gases prior to entering the heated reactor. Momentum and heat-transfer calculations suggested that laminar flow developed as the gases were carried into the heated zone, and the gases quickly warmed to the reaction temperature prior to exiting the (1-in.) tube. Upon exit, the gas jet impinged on the sample in the center of the hot zone of the furnace. The reactor tube was heated with a tube furnace. The reaction byproducts and unreacted gases exited the reactor and were treated in a disposal system constructed from an oil bubbler and three bubblers with ~250–400 mL of 5% sodium hypochlorite. The oil bubbler prevented water and oxygen from diffusing back into the reactor. Hydrazine, a reducing agent, was reacted with sodium hypochlorite, an oxidizing agent, for disposal. The deposition system was also equipped with a vaccum pump that was used for evacuating and backfilling the reactor to remove contaminates prior to reaction. The steady-state temperature inside the reactor was calibrated with a shielded thermometer, IR gun, and temperature indicator wax sticks.

Model Development

Direct growth model

The Deal-Grove model, commonly used for oxidation of silicon, predicts a parabolic relationship between film thickness and reaction time (Sze, 1988). However, this model did not accurately describe the growth of nitride films because the reactant, hydrazine, decomposes resulting in a dramatically slower growth rate with time.

A growth model was also derived by Wu et al. (1982) and simplified by Vogt (1994) that more closely correlated the film thickness vs. growth time relation for the nitridation of silicon. This model provides a useful means of discussing the behavior of this deposition process. The resulting relation can be written as

$$a_i \cdot \sinh(\lambda Z_0) + b_i \cdot [\cosh(\lambda Z_0) - 1] = t \qquad (1)$$

where

$$a_i = \frac{N_i}{k_{\text{int}} C^*}\left[\frac{D_N \cdot \lambda}{h} + \frac{k_{\text{int}}}{D_N \cdot \lambda}\right],$$

$$b_i = \frac{N_i \cdot \lambda}{k_{\text{ink}} C^*}\left[1 + \frac{k_{\text{int}}}{h}\right], \quad \lambda = \sqrt{\frac{k_f}{D_N}}, \quad h = \frac{h_G}{H \cdot k_B \cdot T},$$

D_N is the diffusivity for transport of the reactant across the film; k_f is a first-order rate constant when the reactant is consumed as it is transported across the film; k_{int} is the film/substrate rate constant for the growth of the film; H is Henry's constant; k_B is Boltzmann's constant; T is the absolute temperature; h_G is the gas phase mass-transfer coefficient; C^* is the equilibrium bulk concentration in the nitride film; Z_0 is the thickness of the nitride film; and N_i is the number of nitridants per molecule of the film.

Several simplifications can be made to Eq. 1. For small λZ_0 (k_f is small and D_N is large), the truncated power series relations can be substituted for the hyperbolic functions (Spiegel, 1968). After simplification, the thickness vs. time relation can be written as

$$Z_0^2 + \left(\frac{2 \cdot a_i}{b_i \cdot \lambda}\right) \cdot Z_0 = \left(\frac{2}{b_i \cdot \lambda^2}\right) \cdot t \qquad (2)$$

This parabolic equation is similar to the Deal–Grove model for the oxidation of silicon (Sze, 1988). When the film is very

thin, the second-order term can be neglected, and the film thickness can be written as a linear function of t. This period of growth occurs at short reaction times when the film is thin and the growth rate is controlled by the reaction kinetics. As the film grows, the transport of reactants across the film begins to control the reaction rate. In this case, the first-order term becomes insignificant, and the film thickness can be written as a parabolic function of t.

As λZ_0 becomes larger (k_f is large, D_N is small, and Z_0 is large), the truncated power series approximation is no longer acceptable. In this case, Eq. 1 can be simplified using the exponential relations for the hyperbolic functions (Mindel and Pollack, 1969). Since λZ_0 is large, $e^{-\lambda Z_0} \cong 0$ and Eq. 1 can be simplified as:

$$Z_0 = \frac{1}{\lambda} \cdot \ln\left[\frac{2(t + b_i)}{a_i + b_i}\right]. \tag{3}$$

For large film thicknesses or large λ (that is, k_f is large and/or D_N is small), the growth of the thermal nitride films becomes a logarithmic function of time.

This derivation predicts that the film thickness vs. growth time will have linear-, parabolic-, and logarithmic-shaped regions. When experimental data are compared to the developed relations, the constants, a_i, b_i, and λ can be deduced. Comparison of the constants for various reaction temperatures can help determine the controlling factors of the nitridation reaction.

Chemical vapor deposition model

Two mathematical models were used to study the deposition of boron nitride (BN) from diborane (B_2H_6) and hydrazine (N_2H_4). First, the computer program, SOLGASMIX-PV (Besmann, 1977), was used to calculate the equilibrium composition of the B_2H_6–N_2H_4 CVD system. This program directly minimizes the free energy of the entire reaction system. The equilibrium analysis assumes that the reactions occur in a closed system with an infinite amount of reaction time. The calculations are useful for understanding the feasibility of CVD and direct growth reactions, even though they are typically nonequilibrium processes. The enthalpy and entropy data of possible gaseous, liquid, and solid species for the Ar–B–N–H–O system at 298, 400, 500, 600, 700, 800 and 900 K were used in this case (Lide, 1985; Barin et al., 1977).

Second, a mathematical model describing the momentum and mass transport of the reactants was used. The hot-wall reactor was assumed to be isothermal. Previously, the development of a mathematical model relating the growth characteristics (deposition rate and film composition) to deposition parameters (temperature, reactant concentration, gas flow rate, and reactor geometry) has been helpful for understanding the processes that affect chemical vapor deposition (Wahl, 1977; Wahl, 1984; Vandenbulcke and Vuillard, 1977). Since the flow field could be approximated as stagnation point flow, the equations were simplified similar to the one-dimensional analysis studied for CVD systems by Houtman et al. (1986), Michaelidis and Pollard (1984), and references therein. The partial differential equations were simplified to a set of nonlinear ordinary differential equations that were solved with an iterative finite difference technique (Vogt, 1994).

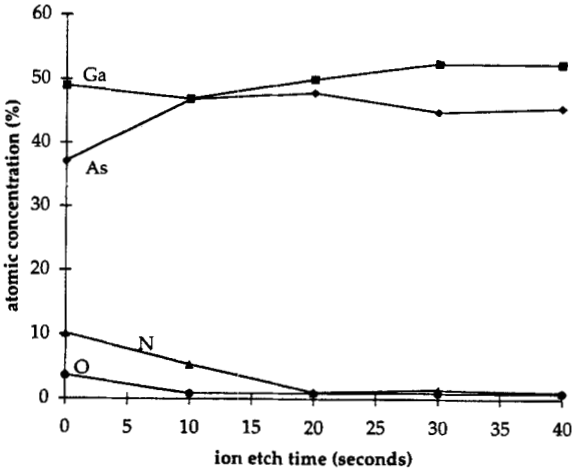

Figure 2. AES depth profile of GaN film grown on GaAs precleaned and nitrided with 99.7% hydrazine at 300°C.

Results and Discussion

Two different kinds of hydrazine reactions will be presented: direct growth and chemical vapor deposition (CVD). During direct growth reactions, hydrazine reacts heterogeneously with the solid phase compound, consuming the surface layers, and forming a metal nitride on the surface. During chemical vapor deposition reactions, gas phase compounds (B_2H_6 and N_2H_4) adsorb and react to form a new material (BN).

Direct growth reactions

GaAs. Nitride growth occurred by exposure to a 1% hydrazine in argon mixture at 200–400°C for one hour. The films were grown by consuming the GaAs surface and forming gallium nitride. Typically, very thin nitride layers on GaAs (< 100 Å) were produced. For example, an AES depth profile of a film grown at 300°C is shown in Figure 2, where the atomic concentration (AES peak-to-peak height corrected by atomic sensitivities (Physical Electronics, 1979) was plotted vs. the ion etch time (proportional to the depth of film). The film was a mixture of nitrogen- and oxygen-containing compounds. The AES results show that the gallium nitride (GaN) films are nonstoichiometric, with the gallium concentration exceeding the nitrogen concentration. The most likely sources of oxygen contamination were incomplete removal of native oxide during precleaning, water impurities in the hydrazine, and oxygen and water contamination of the films during transfer from the dry box to the AES chamber. The higher gallium-to-arsenic ratio shows that arsenic was depleted from the surface film and the semiconductor–film interface. After removal of the film, the gallium and arsenic concentrations were equal. Thus, the film was formed by converting the native semiconductor to gallium oxy-nitride and depleting the region of arsenic, most likely by the formation of arsine.

XPS analysis was used to examine the oxidation state of the elements in the nitride films. The binding energies for the oxidation states of the Ga 3d and N 1s XPS spectra were identified from the literature (Mizokawa et al., 1979). As seen in Figure 3, the N 1s peak is centered at 397.5 eV, which

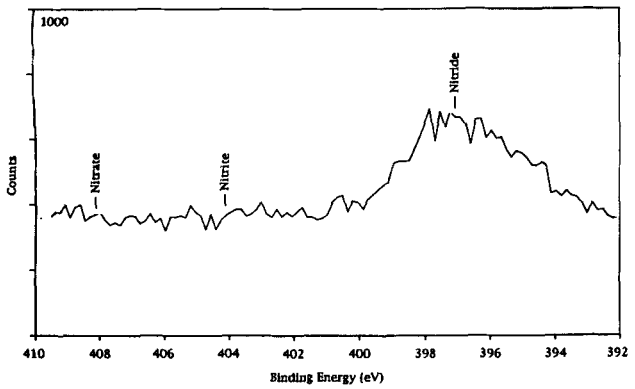

Figure 3. N 1s XPS spectra for GaN film grown on GaAs at 400°C.

corresponds to the nitride oxidation state (Hedman and Martensson, 1980). No peaks were identified at 401 eV or 403 eV, which coincide with nitrite and nitrate, respectively. This shows that the oxidation state of the nitrogen was as the nitrite and not nitrite or nitrate. The Ga 3d spectra in Figure 4 is asymmetric and very broad. It can be fitted with two peaks associated with gallium nitride and gallium oxide. The large peak at 19.5 eV corresponds to gallium nitride, and the small peak at 20.5 eV is gallium oxide. These XPS results show that the films consist primarily of gallium nitride with a small amount of gallium oxide impurity. This suggests that the oxygen impurity remains as an oxide and does not combine with the nitrogen to form a nitrite or nitrate.

The precleaning treatment, cleaning/reaction temperature, and hydrazine purity were investigated in an effort to identify the sources of oxygen contamination, and the results have been discussed elsewhere (Vogt and Kohl, 1993). The results show that removal of the native oxide was important in the final purity of the nitride films. The results also showed that purification of the hydrazine with alumina decreased the amount of oxide in the nitride film, but also resulted in a thinner film. It appears that the water impurity and subsequent oxide content of the film compromises the quality and density of the film, allowing easy penetration of the reactants to the interface.

Silicon. The (100) silicon substrates were phosphorus-doped *n*-type with a carrier concentration of $\sim 1 \times 10^{17}\ \mathrm{cm}^{-3}$.

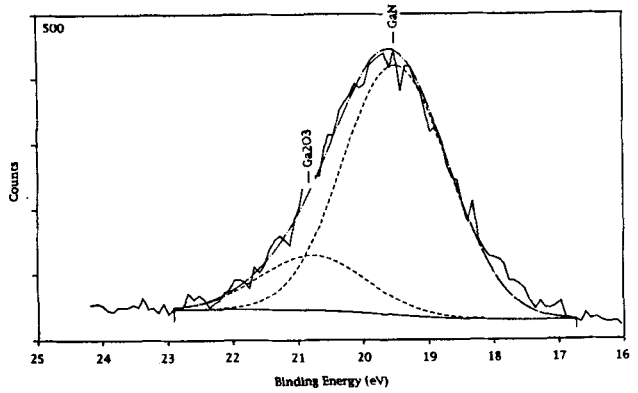

Figure 4. Ga 3d XPS spectra for GaN film grown on GaAs at 400°C.

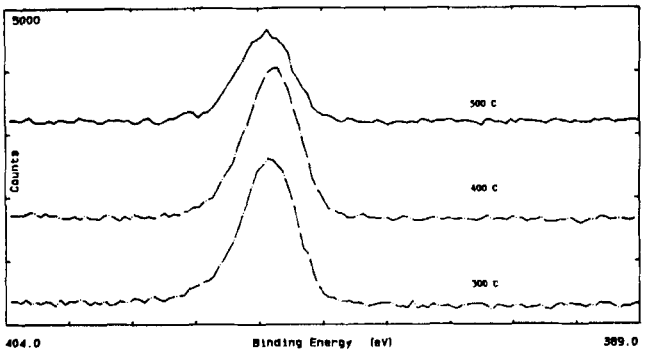

Figure 5. N 1s XPS spectra for silicon nitride films grown at 300, 400 and 500°C.

The samples were cleaned in 5% (vol) HF for 1 min, rinsed in deionized water for 1 min., and blown dry with nitrogen to remove native oxides from the surface. After the HF etch, the samples were introduced into the dry box, placed into the reactor, and reacted in 1% hydrazine (purified with activated alumina) at 300, 400, and 500°C for 0.25–6 h. After reaction, the samples were cooled to ~100–150°C, removed from the reactor, and stored in the dry box for XPS and ellipsometry analysis.

The silicon surfaces were analyzed with XPS, and five elements were identified: silicon (Si 2p-100 eV and Si 2s-200 eV), nitrogen (N 1s-399 eV), oxygen (O 1s-535 eV and O KLL Auger-985 eV), carbon (C 1s-285 eV), and fluorine (F 1s-686 eV and F KLL Auger-885 eV). The carbon and much of the oxygen contaminant probably originated from the adsorption to atmospheric gases like water, oxygen, carbon monoxide, and hydrocarbons during transfer from the reactor to the XPS analysis chamber. The small amount of fluorine remained from the HF etch.

High-resolution XPS scans of the Si 2p, O 1s, N 1s, and C 1s spectra were collected to obtain oxidation state information about the films. The N 1s peak is commonly used for the identification of the nitrogen oxidation state because of its high photoemission intensity (Vasile et al., 1990). As shown in Figure 5, the N 1s XPS spectra for the nitride films grown for 6 h could be interpreted in terms of four singlets located between 396 and 408 eV: nitride (−3 valence state), amine (NH_2 and NH, −1 and −2 oxidation state, respectively), nitrite (+3 oxidation state), and nitrate (+5 oxidation state) (Coyle and Stone, 1964). The binding energy of the N 1s peak for the nitride films grown at 300°C, 400°C, and 500°C all occurred at 397 eV, which corresponds to N^{-3} (that is, nitride). This suggests that the films grown from the decomposition of hydrazine at 300–500°C were silicon nitride.

The Si 2p XPS spectra for the samples grown for 6 h were also measured. The spectra can be interpreted in terms of three nonsymmetrical singlets between 99 and 104 eV associated with Si^0 (99.4 eV), silicon nitride (102 eV), and silicon dioxide (103.5 eV) (Moulder et al., 1992). The Si 2p spectra were very similar for the films grown at 300, 400 and 500°C. The Si 2p peaks had a large peak at 99.4 eV corresponding to Si^0, and a broad peak at 102–104 eV, corresponding to oxidized silicon. The large Si^0 peak was from the silicon substrate. This suggests that the nitride films are thinner than the attenuation length of the photoelectron for silicon (~ 30 Å). The broad peak could be fitted with a combination of

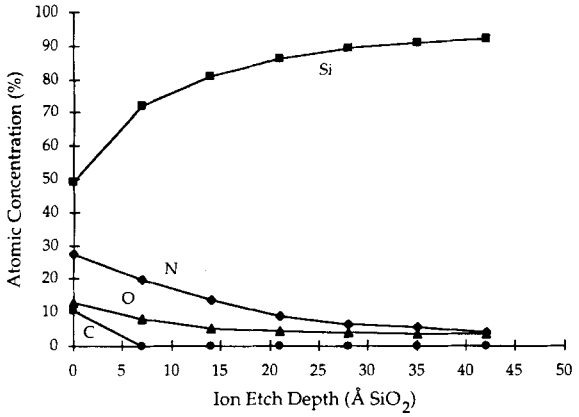

Figure 6. Depth profile of silicon nitride film grown at 300°C.

curves corresponding to silicon nitride and silicon oxide. The silicon nitride peak was the largest and accounted for approximately 75% of the total peak area. The silicon oxide peak was smaller and accounted for only ~ 25% of the total peak area. Since the peak area (intensity) is proportional to the concentration, the Si 2p spectra shows that the films are primarily silicon nitride with a small amount of silicon oxide impurity.

The XPS depth profile was also collected for each film, as shown in Figure 6 for the film grown at 300°C for 6 h. Since the fluorine concentration was small and found only at the surface, it was neglected in the analysis of the films. The results show that the oxygen concentration was less than the nitrogen concentration in the films grown at 300, 400 and 500°C, consistent with the earlier high-resolution XPS results. For the 300°C and 400°C nitride films, the oxygen contamination was found primarily at the surface and likely resulted from the adsorption of water and oxygen during transfer of the sample from the reaction chamber to the XPS analysis chamber. In both cases, the concentration was less than 10%. Meanwhile, the oxygen contamination in the 500°C film was about 17% of the total concentration at the surface, which was higher than found for the 300 and 400°C samples. At 500°C, the increased reaction with oxygen and water contaminants in the reactor may have increased the oxide impurity in the film. Alternatively, the higher reaction temperature may have increased the decomposition rate of the hydrazine, decreasing the amount available for reaction with silicon.

The depth profiles also showed that the thickness of the 300 and 500°C films was roughly equal, ~ 15 Å, but the 400°C film was slightly thicker, ~ 20Å. The transport of reactants across the film might be slightly greater at 400°C than 300°C, increasing the growth rate at the interface. At 500°C, the rate of homogeneous decomposition reaction of hydrazine likely increased and lowered the concentration of hydrazine available for reaction and decreased the growth rate of the film.

The thickness of the nitride films was also measured with ellipsometry as a function of reaction time and temperature. The refractive index of the nitride films was assumed to be 2.0, and the film thickness was calculated from the change in phase and rotation of the polarized light. Table 1 summarizes the results of the ellipsometer measurements. Each point is

Table 1. Silicon Nitride Film Thickness as Function of Reaction Time and Temperature

Reaction Time (s)	300°C Avg. Thickness (Å)	300°C Std. Dev. (Å)	400°C Avg. Thickness (Å)	400°C Std. Dev. (Å)	500°C Avg. Thickness (Å)	500°C Std. Dev. (Å)
900	14.2	0.5	14.0	1.3	—	—
1,080	—	—	—	—	14.6	0.9
1,800	15.4	0.5	—	—	14.9	0.5
2,700	—	—	14.9	1.0	—	—
3,600	15.5	0.7	14.9	1.1	15.0	0.6
10,800	15.4	0.1	14.7	0.6	14.6	0.6
21,600	15.1	0.6	15.6	1.5	15.8	0.5

the average of at least ten measurements. The maximum thickness was approximately 15 ± 5 Å for the films grown at 300, 400, and 500°C. The film thicknesses appear to be similar for the three reaction temperatures. This may result from competition between decomposition and growth reactions. As the temperature increases, the rate of hydrazine decomposition increases, lowering the amount available for film growth. At lower temperatures, the concentration of hydrazine increases (decomposition rate decreases with temperature), but the lower temperatures slow the reaction rate for the film growth. When the average film thickness is plotted vs. the reaction time for each temperature in Figure 7, the points lie close together. Figure 7 also shows that the growth rate was very small after 1 hour of reaction time.

Although the large error in the experiment precluded quantitative analysis of the growth behavior, these results are consistent with the limiting growth model developed earlier. Initially, the film thickness increases as a linear function of time. Eventually, the growth rate slows, and the film thickness increases parabolically with time. Finally, the growth rate becomes very slow and can be estimated as a logarithmic function of time.

The thermal growth model was also used to fit the data for a qualitative analysis of the growth rate. Table 2 shows that the best fit results when a_i and b_i are small. When compared with ammonia reactions at 700–1,100°C, the a_i and b_i constants are more than 4 orders of magnitude smaller. From

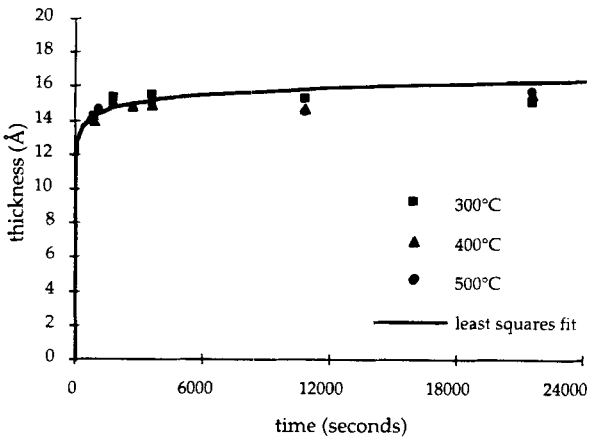

Figure 7. Least-squares fit of nitride growth model for silicon nitride films grown at 300, 400 and 500°C.

Table 2. Fitted Constants for Thermal Nitride Growth Model and Film Thickness after 6 hours of Growth for Hydrazine and Ammonia Reactions

	a_i (s)	b_i (s)	λ ($Å^{-1}$)	6 h Thickness (Å)
Hydrazine 300—500°C	3×10^{-7}	1×10^{-7}	1.55	15
Ammonia 700°C [258]	0.44	2.0	0.41	24
Ammonia 900°C [258]	0.11	0.39	0.28	40
Ammonia 1,100°C [258]	0.024	0.084	0.21	60

Eq. 1, the a_i and b_i constants are inversely proportional to the linear and parabolic growth rate constants, respectively. Since the linear growth region is controlled primarily by reaction kinetics, the small values suggest that the initial nitridation rate is much faster with hydrazine than ammonia.

The results also suggest that the growth rate quickly becomes limited by the transport of the reactive species across the film after the initial layers of the film forms. The growth rate becomes very small, and the film thickness can be described by the logarithmic function of time in Eq. 3. Since a_i and b_i are very small, the logarithmic term changes very slowly with time and is approximately constant. In this case, the thickness vs. time relation is almost flat, and the final thickness is controlled by the $1/\lambda$ term. Since λ is larger at lower temperatures (Table 2), the final film thicknesses are smaller for the films grown in hydrazine at 300–500°C than those grown in ammonia at 700–1,100°C.

Since the diffusivity constant decreases with temperature, λ becomes larger at low temperatures. The diffusion of the reactive species through the film is more difficult. Second, the reaction constant, k_f, is dependent upon the reaction. The reactive species in the hydrazine reaction may decompose or deactivate faster than the reactive species in the ammonia reaction. The resulting k_f (and λ) would be larger for the hydrazine reaction.

Transition Metals. The hydrazine nitridation sequence was also studied on many transition metals to evaluate the applicability of the process. Because surface oxides can affect the hydrazine reactions, the samples were precleaned with acidic etching solutions (Vogt et al., 1994). Following pretreatment, the metal substrates were reacted in 1% hydrazine vapor at 400°C for 1 h. 400°C was chosen for convenience; further reductions in reaction temperature are conceivable, since the reaction is dependent on the decomposition of hydrazine that can occur at lower temperatures.

AES depth profiles showed that the nitride films were successfully grown on Co, Cr, Fe, Mo, Ta, Ti, V, and W. The depth profiles also showed that the films were thin (< 1,000 Å), the nitrogen mole fractions were larger at the surface and decreased in the bulk of the films, and oxygen was the most important contaminant in the films. XPS analysis showed that the films were primarily metal nitrides with small amounts of oxide impurity at the film's surface.

For example, in Figure 8 the N 1s XPS spectra for the nitride film grown on titanium can be analyzed as two peaks: a large peak was found at 397 eV (nitride (Vasile et al., 1990; Wagner et al., 1979)), and a small peak at 399.5 eV was

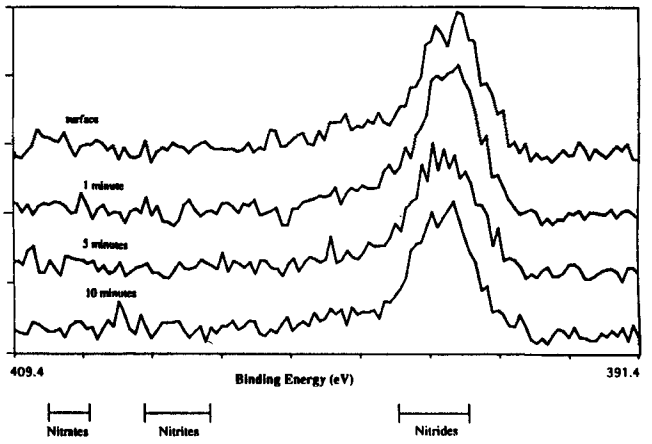

Figure 8. N 1s XPS spectra for the hydrazine-treated titanium sample at the surface and after 1, 5 and 10 min of ion etching.

present on the surface of the film. The peak at 397 eV increased in area, and the peak at 399.5 eV decreased with ion etching. After 10 min of sputtering, the peak at 399.5 eV was no longer observed, but a large peak at 397 eV remained. This suggests that the film is several monolayers thick since a N 1s peak remains after 10 min of ion etching. Hydrazine is not simply adsorbed on the surface. Secondly, Vasille et al. (Raval et al., 1990) showed that a small peak at 399.5 eV results when a nitride film has oxide on the surface. These oxides are removed during ion etching, rendering a single N 1s peak at 397 eV. Thus, the film was a mixture of nitrides and oxides at the surface, and the bulk of the film was primarily a nitride. The effect of oxides on the nitride growth process was investigated more thoroughly and is discussed elsewhere (Vogt et al., 1994).

Chemical vapor deposition reactions

Boron Nitride. A XPS depth profile was used to estimate the thickness and analysis of the chemical composition of a BN film deposited on a GaAs substrate from a 0.39% N_2H_4 and 0.07% B_2H_6 mixture at 400°C for one hour. After correction for the atomic sensitivity and the ion etch rate, the atomic concentration was plotted vs. the depth from the surface as shown in Figure 9. The thickness of the film was approximately 150Å. The film was stoichiometric boron nitride (within the accuracy of XPS). A small oxide impurity was found at the film's surface and at the film/substrate interface. A small amount of oxide impurity was also present in the deposited film, originating from the background water impurity in the hydrazine. The oxygen at the surface most likely resulted from water or oxygen that adsorbed during exposure to air. The interfacial oxide resulted because the native oxides on the GaAs surface were not completely removed prior to deposition of the BN film.

High resolution XPS scans of the N 1s and B 1s spectra were used to determine the oxidation state of elements in the film. The N 1s peak was found at 397.9 eV. This binding energy corresponds to boron nitride (Moulder et al., 1992). The B 1s spectrum were located at 190.5 eV and compare well with BN. Thus, the XPS results show that the film was

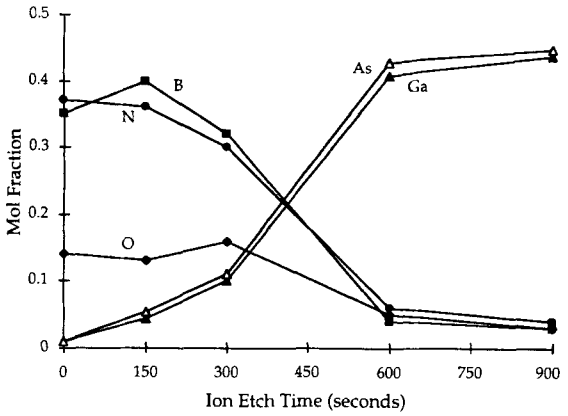

Figure 9. Depth profile for boron nitride film deposited at 400°C.

primarily boron nitride with small amounts of oxide impurity at the surface and the film/substrate interface.

The one-dimensional transport model was used to help evaluate the rate-limiting deposition processes for boron nitride. For kinetically limited reactions, the surface flux is small and $dC/dx \sim 0$ at the surface (very small). When the reaction is transport controlled, dC/dx is very large, and the gas phase concentration of the limiting reagent goes to zero (very small). Thus, the model shows that the transport-limited growth rate for the experimental conditions (0.39% N_2H_4 and 0.07% B_2H_6 at 865 sccm) was predicted to be 3.5×10^6 Å/h. This is several orders of magnitude larger than the actual deposition rate (150 Å/h), suggesting that the deposition rate was limited primarily by kinetics.

To experimentally investigate the effect of temperature on the formation of boron-nitrogen products, a 5% hydrazine in argon mixture and a 781 ppm diborane in argon mixture were warmed separately and mixed at the desired reaction temperature. No solid products formed when solely hydrazine was warmed in the reactor. When only diborane was warmed below 200°C, no visible deposit was found. Above 200°C, a brown, boronlike deposit formed. The brown films were only slightly soluble in concentrated nitric acid and etched from the glass slowly, as expected for boron.

Mixtures of diborane and hydrazine formed compounds more readily. Below 200°C, a thick, white film formed where the reactants combined and mixed. Above 200°C, the white films were not formed, and no visible deposit was found after reaction for 1 h. Chemical analysis of the substrate at 400°C (Figure 9) indicated the formation of thin boron nitride films at higher temperatures.

This shows that the temperature at the point of mixing is critical in determining the final composition of the film. If diborane was warmed above 200°C prior to mixing with hydrazine, it decomposed to boron. This was undesirable because the diborane reactant was being depleted prior to reaching the target sample. When hydrazine and diborane were mixed at temperatures below 200°C, reactions occurred between the electrophilic diborane and the nucleophilic hydrazine that produced white-colored solid complexes and adducts. At higher temperatures (> 200°C), the adducts and complexes rearranged and formed boron nitride products.

In the extreme experimental cases, these results qualitatively agreed with the chemical equilibrium predictions (Vogt, 1994). A gas mixture of hydrazine with excess diborane was predicted to pyrolyze into a mixture of boron and boron nitride. Experimentally, when the gas stream was solely diborane, the film was primarily boron. Alternatively, the equilibrium calculations predict that boron nitride films will form when the mixture contains excess hydrazine (Vogt, 1994). Experimentally, at higher reaction temperatures (400°C), stoichiometric boron nitride films were formed. At lower reaction temperatures (< 200°C), the equilibrium predictions failed because the kinetics for the dehydrogenation of the diborane–hydrazine complex appeared to limit the formation of boron nitride, that is, boron–nitrogen adducts formed.

The results also agreed with previous results. A Lewis acid–base reaction readily occurs between electrophilic diborane and nucleophilic hydrazine. These reactions often lead to a large number of ionic and covalent complexes and adducts, especially below 200°C (Coyle and Stone, 1964; Goubeau and Richter, 1961; Niedenzu and Dawson, 1965; Noth, 1970). At higher temperatures, the adducts either decompose into hydrazine and diborane or undergo rearrangement and form different compounds (Goubeau and Richter, 1961; Stock, 1933). For example, hydrazinolysis of aminoboranes with free hydrazine can yield ringlike and other addition compounds that are often gaseous above 200°C. These products are similar to those found when ammonia and diborane are combined, where the adducts decompose above 200°C to yield compounds such as $B_3N_3H_6$, $NH_2B_2H_5$, and $B_2(NH_3)$ (Niedenzu and Dawson, 1965). Complete dehydrogenation can also occur, and boron nitride films will form.

Conclusion

The direct nitridation of gallium arsenide with hydrazine at 200–400°C to produce gallium nitride has been demonstrated. The films were grown by consuming the gallium arsenide substrate and depleting the surface region of arsenic. The films contained some oxygen impurities, but the quality of the films was improved with removal of the native oxide and by purifying the hydrazine.

Nitride films were grown on silicon with hydrazine at 300–500°C. The initial growth rates with hydrazine are much faster than the growth rates with ammonia. The results also suggest that the growth rate becomes transport-limited quickly, and the film thickness plateaus at approximately 15 Å when the reaction temperatures are 300–500°C.

Metal nitride films were formed on Co, Cr, Fe, Mo, Si, Ta, Ti, V, and W by thermal nitridation with hydrazine at 400°C. An oxide impurity was found in each film. On titanium, the film is several monolayers thick since an N 1s XPS peak remains after 10 min of ion etching.

The atmospheric chemical vapor deposition of boron nitride from diborane and hydrazine was demonstrated. The temperature was critical in determining the final composition of the film. When diborane was warmed above 200°C, boron films were deposited. Below 200°C, decomposition was not observed. When mixtures with excess hydrazine were reacted below 200°C, white-colored adducts formed. Adduct formation was not observed when the mixture was heated above 200°C. When a 0.39% hydrazine/0.07% diborane mixture was

heated to 400°C, the mixture reacted heterogeneously on the substrate surface, and a stoichiometric film of boron nitride was deposited.

Literature Cited

Adams, A. C., and C. D. Capio, "The Chemical Deposition of Boron-Nitrogen Films," *J. Electrochem. Soc.*, **127**, 399 (1980).

Adams, A. C., "Characterization of Films Formed by Pyrolysis of Borazine," *J. Electrochem. Soc.*, **128**, 1378 (1981).

Barin, I., O. Knacke, and O. Kubaschewski, *Thermochemical Properties of Inorganic Substances: Supplement*, Springer-Verlag, New York (1977).

Berger, A., D. Troost, and W. Monchs, "Adsorption of Atomic Nitrogen at Gallium Arsenide (110) Surfaces," *Vacuum*, **41**, 669 (1990).

Besmann, T. M., "ORNL/TM-5775," Oak Ridge National Laboratory, Oak Ridge, TN (1977).

Blanchet, R., C. Santinelli, J. Chave, M. Garrigues, S. Krawczyk, and P. Viktorovitch, "Large Surface Fermi Level Shift in High Temperature Annealed Metal-Insulator-Gallium Arsenide Structures Prepared in Presence of Oxygen," *J. Vac. Sci. Tech. B*, **2**, 681 (1984).

Capasso, F., and G. F. Williams, "A Proposed Hydrogenation/Nitridation Passivation Mechanism for Gallium Arsenide and Other III-V Semiconductor Devices," *J. Electrochem. Soc.*, **129**, 821 (1982).

Chang, R. P. H., T. T. Sheng, C. C. Chang, and J. J. Coleman, "The Effect of Interface Arsenic Domains on the Electrical Properties of Gallium Arsenide MOS Structures," *Appl. Phys. Lett.*, **33**, 341 (1978).

Coyle, A., and J. Stone, *Progress in Boron Chemistry*, H. Steinberg and R. McCloskey, eds., Pergamon, New York (1964).

Crowl, D. A., and J. F. Louvar, *Chemical Process Safety, Fundamentals with Applications*, Prentice-Hall, Englewood Cliffs, NJ (1990).

Faulkner, K. R., D. K. Wickenden, B. J. Isherwood, B. P. Richards, and I. H. Scobey, "Gallium Nitride Formed by Vapor Deposition and by Conversion from Gallium Arsenide," *J. Mat. Sci.*, **5**, 308 (1970).

Frese, K. W., Jr., and S. R. Morrison, "Electrochemical Measurements of Interface States at the Gallium Arsenide/Oxide Interface," *J. Electrochem. Soc.*, **126**, 1235 (1979).

Friedel, P., and J. P. Landesman, "Photoemission Study of the Passivation of Gallium Arsenide in a Nitrogen Multipolar Plasma," *Philos. Mag. B*, **55**, 711 (1987).

Gafri, O., A. Grill, D. Itzhak, A. Inspection, and R. Avni, "Boron Nitride Coatings on Steel and Graphite Produced with a Low Pressure rf Plasma," *Thin Solid Films*, **72**, 523 (1980).

Good, C. D., and D. R. Poole, U.S. Patent 3 598 546 (1971).

Goubeau, J., and E. Richter, "Preparation of Boron-Nitrogen Adducts," *Z. Anorg. Allg. Chem.*, **310**, 123 (1961).

Gourrier, S., L. Smit, P. Friedel, and P. K. Larsen, "Photoemission Studies of Molecular Beam Epitaxially Grown Gallium Arsenide (001) Surfaces Exposed to a Nitrogen Plasma," *J. Appl. Phys.*, **54**, 3993 (1983).

Gourrier, S., P. Friedel, and P. K. Larsen, "Core Level Photoemission Study of the Interaction of Plasmas with Real Gallium Arsenide (100) Surfaces," *Surf. Sci.*, **152/153**, 1147 (1985).

Guizot, J., P. Alnot, J. Perrin, and B. Allain, "Modeling of UV-CVD Deposition of Silicon Nitride," *Mat. Res. Soc. Symp. Proc.*, **144**, 513 (1989).

Hall, M., M. F. Rau, and J. W. Evans, "Microstructural Aspects of Gas-Solid Reactions," *J. Electrochem. Soc.*, **133**, 1934 (1986).

Hedman, J., and N. Martensson, "Gallium Nitride Studied by Electron Spectroscopy," *Phys. Scr.*, **22**, 176 (1980).

Houtman, C., D. B. Graves, and K. F. Jensen, "CVD in Stagnation Point Flow. An Evaluation of the Classical 1d Treatment," *J. Electrochem. Soc.*, **133**, 961 (1986).

Hyder, S. B., and T. O. Yep, "Structure and Properties of Boron Nitride Films Grown by High Temperature Reactive Plasma Deposition," *J. Electrochem. Soc.*, **123**, 1721 (1976).

Isherwood, B. J., and D. K. Wickenden, "Preparation of Single-Phase Gallium Nitride from Single-Crystal Gallium Arsenide," *J. Mat. Sci.*, **5**, 869 (1970).

Kang, C. H., K. Kondo, J. Lagowski, and H. C. Gatos, "Arsenic Ambient Conditions Preventing Surface Degradation of Gallium Arsenide during Capless Annealing at High Temperatures," *J. Electrochem. Soc.*, **134**, 1261 (1987).

Kim, C., B. K. Sohn, and K. Shono, "Chemical Vapor-Deposited Boron Nitride Film on Silicon as a Boron Diffusion Source," *J. Electrochem. Soc.*, **131**, 1384 (1984).

King, P. L., L. Pan, P. Pianetta, A. Shimkunas, P. Mauger, and D. Seligson, "X-Ray Induced Damage in Boron Nitride, Silicon, and Silicon Nitride Lithography Masks," *J. Vac. Sci. Tech. B*, **5**, 257 (1987).

Lee, J. S., C. S. Park, J. Y. Kang, and D. S. Ma, "Characterization of Ion-beam Deposited Refractory Tungsten Nitride Films on Gallium Arsenide," *J. Vac. Sci. Tech.*, **B8**, 1117 (1990).

Levy, R. A., D. J. Resnick, R. C. Frye, A. W. Yanof, G. M. Wells, and F. Cerrina, "Characterization of Boron Nitride Electron Lithography Masks," *J. Vac. Sci. Tech. B*, **6**, 162 (1988).

Lide, D. R., Jr., ed., *Janaf Thermochemical Tables*, Amer. Chem. Soc. and Amer. Inst. of Physics for Nat. Bur. of Stand. (U.S.), p. 14 (1985).

Maissel, L. I., and R. Glang, eds., *Handbook of Thin Film Technology*, McGraw-Hill, New York (1970).

Matsuno, Y., K. Matsushita, T. Hariu, and Y. Shibata, "Low Temperature Thermal Nitridation of Gallium Arsenide Surfaces," *Japan. J. Appl. Phys.*, **19**, 6383 (1980).

Michaelidis, M., and R. Pollard, "Analysis of Chemical Vapor Deposition of Boron," *J. Electrochem. Soc.*, **131**, 860 (1984).

Mindel, M. J., and S. R. Pollack, "Effect of Metal Vacancies on the Oxidation Kinetics of Metals," *Acta Met.*, **17**, 1441 (1969).

Mizokawa, Y., H. Iwasaki, R. Nishitani, and S. Nakamura, "An XPS Analysis of the Oxide Films on Gallium Arsenide," *J. Electrochem. Soc.*, **126**, 1370 (1979).

Motojima, S., Y. Tamura, and K. Sugiyama, "Low Temperature Deposition of Hexagonal Boron Nitride Films by Chemical Vapor Deposition," *Thin Solid Films*, **88**, 269 (1982).

Moulder, J. F., W. F. Stickle, P. E. Sobol, and K. D. Bomben, *Handbook of Photoelectron Spectroscopy*, Perkin-Elmer Corp., Eden Prairie, MN (1992).

Murarka, S. P., C. C. Chang, and A. C. Adams, "Thermal Nitridation of Silicon in Ammonia Gas: Composition and Oxidation Resistance of the Resulting Films," *J. Electrochem. Soc.*, **126**, 996 (1979a).

Murarka, S. P., C. C. Chang, D. N. K. Wang, and T. E. Smith, "Effect of Growth Parameters on the Chemical Vapor Deposition (CVD) of Boron Nitride and Phosphorus-Doped Boron Nitride," *J. Electrochem. Soc.*, **126**, 1951 (1979b).

Nakamura, K., "Preparation and Properties of Amorphous Boron Nitride Films by Molecular Flow Chemical Vapor Deposition," *J. Electrochem. Soc.*, **132**, 1757 (1985).

Nakamura, K., "Preparation and Properties of Boron Nitride Films by Metal-Organic Chemical Vapor Deposition," *J. Electrochem. Soc.*, **133**, 1120 (1986).

Niedenzu, K., and J. Dawson, *Boron-Nitrogen Compounds*, Academic Press, New York (1965).

Noth, A., *Progress in Boron Chemistry*, Vol. 3, R. Brotherton and H. Steinberg, eds., Pergamon, New York (1970).

Pankove, J., "Passivation of Gallium Arsenide Surfaces," Air Force Office of Scientific Research Rep. AFOSR-TR-80-1029, AD-A090512 (1980).

Pankove, J. I., J. E. Berkeyheiser, S. J. Kilpatrick, and C. W. Magee, "Passivation of Gallium Arsenide Surfaces," *J. Electron. Mat.*, **12**, 359 (1983).

Physical Electronics by Model 600, Scanning Auger Multi-Probe Computer Database (1979).

Prochazkova, O., and F. Srobar, "Correlation between Preparation Variables and Dielectric Data of Gallium Nitride Formed by Gallium Arsenide Conversion," *Krist. Tech.*, **12**, 1293 (1977).

Rand, M. J., and J. F. Roberts, "Preparation and Properties of Thin Film Boron Nitride," *J. Electrochem. Soc.*, **115**, 423 (1968).

Raval, R., M. Harrison, and D. King, *The Chemical Physics of Solid Surfaces and Heterogeneous Catalysis*, Vol. 3, *Chemisorption Systems, Part A*, D. King and D. Woodruff, eds., Elsevier, New York (1990).

Rodriguez, J. A., C. M. Truong, J. S. Corneille, and D. W. Goodman, "Molecular Precursors to Boron Nitride Thin Films: 1. Adsorption of Diborane on Ruthenium (0001), Ammonia/Ruthenium (0001),

and Oxygen /Ruthenium (0001) Surfaces," *J. Phys. Chem.*, **96**, 334 (1992).
Runyan, W. R., and K. E. Bean, *Semiconductor Integrated Circuit Processing Technology*, Addison-Wesley, Reading, MA (1990).
Sano, M., and M. Aoki, "Chemical Vapor Deposition of Thin Films of Boron Nitride onto Fused Silica and Sapphire," *Thin Solid Films*, **83**, 247 (1981).
Sawada, T., H. Hasegawa, and H. Ohno, *Proc. Symp. on Dielectric Films on Compound Semiconductors*, V. J. Kapoor, ed., Electrochemical Society, Honolulu, HI, p. 17 (1987); Pennington, NJ (1988).
Schmidt, E. W., *Hydrazine and Its Derivatives, Preparation, Properties, Applications*, Wiley, New York (1984).
Schwartz, G. P., G. J. Gualtieri, G. W. Kammlott, and B. Schwartz, "An X-Ray Photoelectron Spectroscopy Study of Native Oxides on Gallium Arsenide," *J. Electrochem. Soc.*, **126**, 1737 (1979).
Spiegel, M. R., *Mathematical Handbook, Schaum's Outline Series*, McGraw-Hill, New York (1968).
Stock, A., *Hydrides of Boron and Silicon*, Cornell Univ. Press, London (1933).
Sze, S. M., *VLSI Technology*, 2nd ed., McGraw-Hill, New York (1988).
Thurmond, C. D., G. P. Schwartz, G. W. Kammlott, and B. Schwartz, "Low Temperature Synthesis of Boron Nitride from Condensed Diborane and Ammonia Using Synchrotron Radiation," *J. Electrochem. Soc.*, **127**, 1366 (1980).
Troost, D., H. Baier, A. Berger, and W. Monch, "Nitride Layers on Gallium Arsenide (110) Surfaces," *Surf. Sci.*, **242**, 324 (1991).
Truong, C. M., J. A. Rodriguez, and D. W. Goodman, "Molecular Precursors to Boron Nitride Thin Films. 2. Coadsorption and Reaction of Hydrazine and Diborane on Ruthenium (0001) Surfaces," *J. Phys. Chem.*, **96**, 341 (1992).
Vasile, M. J., A. B. Emerson, and F. A. Baiocchi, "Growth and Characterization of Thin Titanium Nitride Films," *J. Vac. Sci. Tech.*, **A8**, 99–105 (1990).
Vandenbulcke, L., and G. Vuillard, "Mass Transfer, Equilibrium, and Kinetics in the Chemical Vapor Deposition of Boron from Impinging Jets," *J. Electrochem. Soc.*, **124**, 1931 (1977).
Vogt, K. W., and P. A. Kohl, "Gallium Arsenide Passivation through Nitridation with Hydrazine," *J. Appl. Phys.*, **74**, 6448 (1993).
Vogt, K. W., L. A. Naugher, and P. A. Kohl, "Nitridation of Transition Metals with Hydrazine," *Thin Solid Films*, **256**, 106 (1994).
Vogt, K. W., "Nitridation Reactions with Hydrazine," PhD Thesis, Georgia Institute of Technology, Atlanta (1994).
Wagner, C. D., W. M. Riggs, L. E. Davis, J. F. Moulder, and G. E. Muilenburg, eds., *Handbook of X-Ray Photoelectron Spectroscopy*, Perkin-Elmer Corp., Eden Prairie, MN (1979).
Wahl, G., "Hydrodynamic Description of CVD Processes," *Thin Solid Films*, **40**, 13 (1977).
Wahl, G., "Increasing the Wear Resistance, Corrosion Resistance, and Fatigue Strength by Nitriding," *Chemical Vapor Deposition 1984*, The Electrochemical Soc. Softbound Proceedings Series, Vol. 84–86, Pennington, NJ (1984).
Wang, X., A. Reyes-Mena, and D. Lichtman, "Interface Composition Studies of Thermally Oxidized Gallium Arsenide Using Auger Depth Profiling," *J. Electrochem. Soc.*, **129**, 851 (1982).
Weast, R. C., ed., *CRC Handbook of Chemistry and Physics*, 61st ed., CRC Press, Boca Raton, FL (1980).
Wu, C. Y., C. W. King, M. K. Lee, and C. T. Chen, "Growth Kinetics of Silicon Thermal Nitridation," *J. Electrochem. Soc.*, **129**, 1559 (1982).

Manuscript received Aug. 2, 1994, and revision received Dec. 9, 1994.